Perfect quintuple layer Bi_2Te_3 nanowires: Growth and thermoelectric properties

P. Schönherr, D. Kojda, V. Srot, S. F. Fischer, P. A. van Aken, and T. Hesjedal

Citation: APL Materials **5**, 086110 (2017); doi: 10.1063/1.4986524
View online: http://dx.doi.org/10.1063/1.4986524
View Table of Contents: http://aip.scitation.org/toc/apm/5/8
Published by the American Institute of Physics

Perfect quintuple layer Bi_2Te_3 nanowires: Growth and thermoelectric properties

P. Schönherr,[1] D. Kojda,[2] V. Srot,[3] S. F. Fischer,[2] P. A. van Aken,[3] and T. Hesjedal[1,a]

[1]*Clarendon Laboratory, Department of Physics, University of Oxford, Oxford OX1 3PU, United Kingdom*

[2]*Humboldt-Universität zu Berlin, Newtonstr. 15, 12489 Berlin, Germany*

[3]*Stuttgart Center for Electron Microscopy, Max Planck Institute for Solid State Research, Heisenbergstr. 3, 70569 Stuttgart, Germany*

(Received 5 June 2017; accepted 9 August 2017; published online 23 August 2017)

Bi_2Te_3 nanowires are promising candidates for thermoelectric applications. Vapor-liquid-solid growth of these nanowires is straightforward, but the traditional Au-catalyzed method is expected to lead to Au contamination and subsequently crystal defects. Here, we present a comparison of the Au-catalyzed growth method with an alternative method using TiO_2. We observe that the latter approach results in perfect quintuple layer nanowires, whilst using Au leads to mixed quintuple and septuple layer structures. Despite these differences, we surprisingly find only a negligible effect on their thermoelectric properties, namely conductivity and Seebeck coefficient. This result is relevant for the further optimization and engineering of thermoelectric nanomaterials for device applications. [http://dx.doi.org/10.1063/1.4986524]

The efficiency of thermoelectric (TE) materials is quantified by the figure of merit $ZT = S^2\sigma T/\kappa$, a function of the temperature T, the Seebeck coefficient S, the electrical conductivity σ, and the thermal conductivity κ. Bi_2Te_3 is a TE material with a naturally high ZT and it is a topological insulator (TI).[1,2] The high ZT of Bi_2Te_3 is supported by poor thermal conductivity due to heavy atoms and good electrical conductivity due to the topological surface states. It can be further improved by using low-dimensional structures such as nanowires.[3,4] One obstacle on the road to efficient thermoelectric Bi_2Te_3 nanowires is a high intrinsic doping by antisite defects, which can be reduced through annealing.[5,6] Here, we demonstrate how to control the crystal structure of Bi_2Te_3 nanowires through the choice of catalyst, and we present measurements of the basic thermoelectric properties.

Sample growth. Bi_2Te_3 nanostructures were grown on Si(100) substrates by vapor transport in a Nabertherm B180 horizontal 1 in.-diameter tube furnace (Lilienthal, Germany). The precursor was made by crushing Bi_2Te_3 crystals into a fine powder. It was loaded into the center of the furnace and evaporated by heating.[7] The vapor was transported by a N_2 carrier gas from the hot center of the furnace (600 °C) 22.5 cm towards the cold end to a location with a temperature of 500 °C, where the Si substrates were placed. The Si substrates were coated with poly-L-lysine. A 1:10 diluted solution was pipetted onto the substrate and left for 3 min. Then it was flushed with de-ionized water and dried. Catalyst nanoparticles were deposited on top of these substrates. Au nanoparticles with 5 nm diameter (commercially available from Nanocs) were applied in a 1:10 solution for 3 min and flushed with de-ionized water. TiO_2 nanoparticles with 20 nm diameter were applied from a custom-made solution with de-ionized water and flushed after 3 min. All substrates were blow dried to remove any water. The Au-catalyzed sample was grown at a gas flow of 150 SCCM and the TiO_2-catalyzed sample was grown at 300 SCCM. After loading the substrates the tube was flushed by N_2 and pumped for

[a]Author to whom correspondence should be addressed: Thorsten.Hesjedal@physics.ox.ac.uk

15 min. Then the furnace was ramped up to growth temperature over 1 h (ramp rate ~10 °C/min), and the temperature was held constant for 1 h. The furnace cooled down naturally after the growth cycle was finished. Then, the substrates were removed from the cold furnace and analyzed using scanning electron microscopy (SEM; Jeol JSM-6610LV) and energy-dispersive X-ray spectroscopy (EDX; Jeol JSM-6610LV). Note that in the following, we will for simplicity refer to the nanostructures and sub-micron sized belts or ribbons as nanowires.

Electron microscopy. Individual nanowires were picked by hand using a microtool (wedge shape) and transferred onto a clean Si wafer. The sample was placed flat on the surface for preparation in cross-sectional geometry using focused ion beam (FIB; FEI Quanta 600 FEG with Ga ions). High-angle annular dark-field scanning transmission electron microscopy (HAADF-STEM) and energy-dispersive X-ray spectroscopy (EDX-STEM) were carried out at 200 kV on a JEOL ARM200F (JEOL Co., Ltd.), equipped with a cold field-emission gun and a DCOR probe Cs corrector (CEOS Co., Ltd.) to resolve the atomic structure. EDX data were obtained using a 100 mm^2 JEOL Centurio SDD-EDX detector (JEOL Co., Ltd.) and the Thermo Noran System 7 EDX system (Thermo Fisher Scientific Inc.). The STEM data were analyzed using Digital Micrograph (Gatan Inc.) and for HAADF-STEM image noise removal a multivariate statistical analysis plug-in (HREM Research Inc.) and a script function written by Mitchell were used.[8]

Thermoelectric characterization. For TE characterization, individual nanowires are transferred from the as-grown substrate to a TE characterization platform using an indium tip.[9] They are placed on the platform so that they bridge a micron-sized gap (~7 μm wide) between two symmetric, free-standing cantilevers and can be contacted by four Pt electrodes of which two electrodes serve as thermometers on the cantilevers. The electrodes are ~3 μm wide and the gap between paired electrodes is ~2 μm. More details about the setup can be found in Wang *et al.*[10] The section of the nanowire overlapping the Pt contacts is covered by a layer of Pt and C using electron beam induced deposition in a Nova 600 NanoLab (FEI) to guarantee mechanical stability and ohmic contacts. The deposition parameters used to reduce the halo effect were 10 kV acceleration voltage, specimen current 0.54 nA, and a dwell time of 1 μs, which have been shown to give good ohmic contacts to Bi_2Te_3.[4] A further improvement of the electric contacts could be achieved by replacing Pt with Au.[11] The electrical conductivity can be extracted by four-point-probe measurements. The Seebeck coefficient is measured using dedicated heating electrodes on the cantilevers by measuring the voltage over the gap and the resistance change of the thermometers. A description of the measurement process is given by Kojda *et al.*[12] The length, width, and height of each measured nanowire are obtained from SEM images (Gemini SEM 500) taken at different tilts.

The phenomenological difference between Bi_2Te_3 nanowires catalyzed by TiO_2 and catalyzed by Au is shown in Fig. 1. The two samples differ mainly with respect to the width of the nanowires. The TiO_2-catalyzed sample which is shown in Fig. 1(a) is characterized by broad, ribbon-like nanowires. Most of the nanostructures on the sample are small plates with a diameter around 1 μm and occasionally up to 10 μm. The Au-catalyzed sample is characterized by a lower yield and thinner nanowires, as shown in Fig. 1(b). Figure 1(c) presents the diameter of 103 nanowires (39 for Au- and 70 for TiO_2-catalyzed growth) as a function of length. It is known from side-view imaging that there is very little tilt of the nanowires with respect to the substrate, but we cannot exclude that these top-view diameter (i.e., width) measurements are underestimations. The same argument can be applied to the length measurements of the nanowires. The two samples show a similar trend with low diameter nanowires growing to arbitrary length up to 54 μm. Most nanowires are in the diameter-window up to 1.5 μm. Diameters above 1.5 μm were only observed for TiO_2-catalyzed nanowires. The diameter distribution below 1 μm is very similar between Au-catalyzed and TiO_2-catalyzed nanowires, as can be seen in the inset in Fig. 1(c).

We found previously that small Au-catalyzed $Bi_2(Se,Te)_3$ nanowires grow by the vapor-liquid-solid mechanism.[13] The functioning of the TiO_2 catalyst particle remains rather elusive beyond the initial nucleation stage.[7] The findings above suggest identical growth mechanisms for thin nanowires given the identical distribution at low diameters. This supports the idea of self-catalyzed growth from a liquid Te-particle in case of the presence of TiO_2 nanoparticles similar to Au-catalyzed growth.[7] The diameter of Au-catalyzed nanowires is confined below 1.5 μm, whereas TiO_2-catalyzed growth can also lead to rather broad belts whose growth mechanism was analyzed earlier.[7]

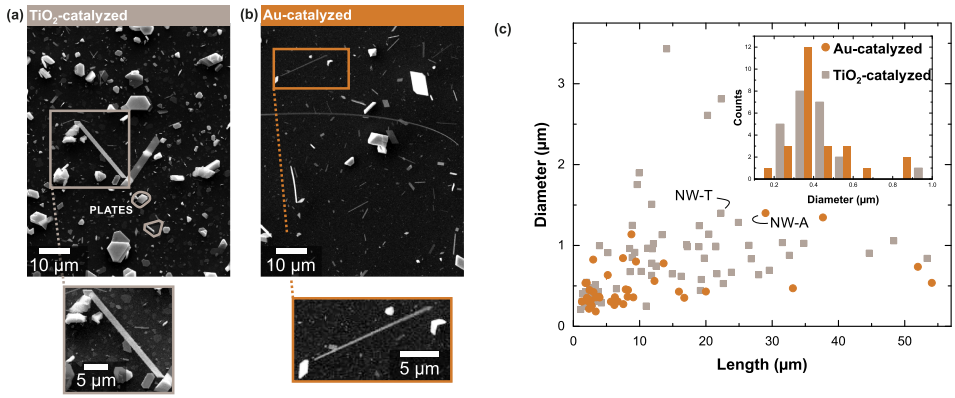

FIG. 1. (a) Top-view SEM image of an as-grown sample of TiO_2-catalyzed Bi_2Te_3 nanowires. A large and a small nanowire are indicated. Plates are encircled in gray. The area of the gray rectangle is enlarged in the inset and shows a broad nanowire. (b) SEM image of an as-grown sample of Au-catalyzed Bi_2Te_3 nanowires. The area of the orange rectangle is enlarged in the inset and shows a thin nanowire. (c) Diameter versus length of Bi_2Te_3 nanowires measured from the SEM pictures of the as-grown samples. Au-catalyzed Bi_2Te_3 nanowires are thinner than TiO_2 catalyzed Bi_2Te_3 nanowires. Note, that SEM top-view length measurements underestimate the true length since nanowires mostly grow at an angle to the substrate.

It is well-known that Au-catalyzed nanowire growth leads to catalyst contamination and undesired doping of Au atoms into the crystalline matrix of the material.[14,15] Cross sections of both types of nanowires, as illustrated in Fig. 2(a), were prepared by FIB perpendicularly to the long axis of the wire in order to confirm a potential impact of the choice of catalyst on the crystal structure. The cross section of the TiO_2-catalyzed nanowire is shown in Fig. 2(b), and the cross section of the Au-catalyzed nanowire is shown in Fig. 2(c). The latter is significantly thicker than the former but their width is nearly identical. The ribbons grow along the [110]-direction, so that the cross section maps to the atomic arrangement shown in Fig. 2(d). We refer to Schönherr *et al.* for a more detailed description of the growth direction of Bi_2Te_3 nanowires.[7] The TiO_2-catalyzed nanowire consists purely of quintuple layers, as shown in Fig. 2(e), whereas the Au-catalyzed nanowire contains septuple layers and quintuple layers, as shown in Fig. 2(f).

Such septuple layer structures were first observed in MBE-grown Bi_2Te_3 thin films[16] and appear in template-assisted Bi_2Te_3 nanowires as local, "connecting" patches between two defective quintuple layer structures.[17] Typically, a septuple layer is not wider than a few nm before it splits.[16]

The question is whether the choice of the catalyst has a measurable impact on the power factor of Bi_2Te_3 nanowires including the electric conductivity and the Seebeck coefficient. In order to answer this question, we will characterize the TiO_2-catalyzed Bi_2Te_3 nanowire shown in Fig. 3(a) and the Au-catalyzed Bi_2Te_3 nanowire shown in Fig. 3(b). The dimensions of each of the two nanowires are shown in Fig. 3(c). The TiO_2-catalyzed nanowire is only half the length (probed part between the electrodes) and cross-sectional area of the Au-catalyzed nanowire. In terms of the electric conductivity, we find $(2.0 \pm 0.1) \times 10^4$ S/m for the Au-catalyzed sample and $(1.6 \pm 0.2) \times 10^4$ S/m for the TiO_2-catalyzed sample at room temperature, respectively. The given errors are mainly based on the errors associated with measurement of the geometry (e.g., the width and height are (249 ± 9) nm and (110 ± 13) nm for a typical wire), whereas the resistance can be measured with a much higher precision. The value for the TiO_2-catalyzed nanowire is close to intrinsic bulk samples at 1.4×10^4 S/m and similarly low as reported previously.[12,18,19] The Au-catalyzed nanowire has a 25% higher conductivity.

A similar variation has been observed on samples within an identical batch by Kojda *et al.*, and it can be attributed to variation in the number of antisite defects which act as donors.[20] The septuple layer defects observed here are likely to act as acceptors with Bi (3+) and Te (2−) counteracting n-type behavior.[16] Au (1+) doping in the form of antisite defects, vacancies, and interstitial doping, which is an expected side effect of the use of Au catalyst particles, potentially also acts as an acceptor and decreases the conductivity.[14,21] Au contamination of the sidewalls by the catalyst contributes to an increase of the conductivity as well.[15]

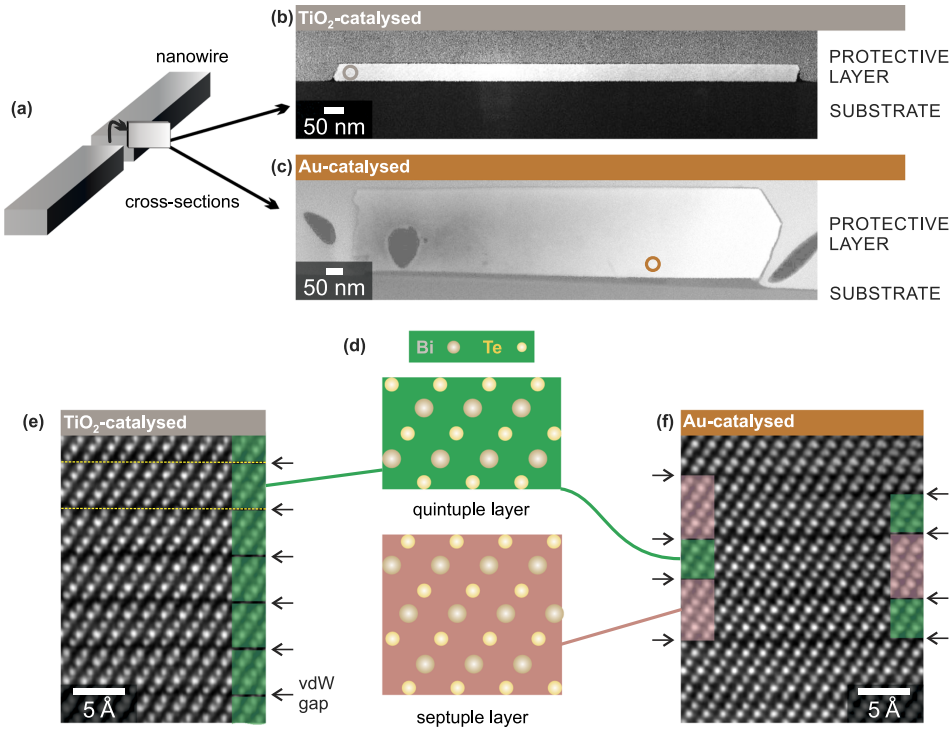

FIG. 2. (a) Sketch of a cross section taken from a Bi_2Te_3 nanowire. The cross section is taken perpendicularly to the long axis. (b) HAADF-STEM image of a cross section taken from a TiO_2-catalyzed Bi_2Te_3 nanowire. A circle indicated the location of the high-resolution scan. (c) HAADF-STEM image of a cross section taken from an Au-catalyzed Bi_2Te_3 nanowire. Dark holes are caused by thinning the samples through ion milling. A circle indicated the location of the high-resolution scan. (d) Crystal structure of Bi_3Te_4 (septuple layer) and Bi_2Te_3 (quintuple layer) viewed from the ⟨110⟩ direction. (e) HAADF-STEM high-resolution image of the crystal structure of a Bi_2Te_3 nanowire [as indicated in (b)] grown using TiO_2 catalyst particles. The crystal structure consists of perfect quintuple layers (green rectangles). The van der Waals gaps are indicated (black arrows). (f) HAADF-STEM high-resolution image of the crystal structure of a Bi_2Te_3 nanowire [as indicated in (c)] grown using Au catalyst particles. The crystal structure consists of septuple and quintuple layers in a random order.

In summary, the overall effect of defects in the Au-catalyzed nanowire is to increase the conductivity compared to the TiO_2-catalyzed sample. The difference, however, is small and within the variation of a batch of 'identical' samples. The Seebeck coefficients relative to Pt (negligible Seebeck coefficient) are (-114.5 ± 0.4) μV/K at 296 K (Au-catalyzed) and (-120.5 ± 0.4) μV/K at 293 K (TiO_2-catalyzed). Note that the thermoelectric measurements were only carried out on two individual nanowires.

The absolute values are more than two times as high compared to previously reported as-grown $Bi_{0.39}Te_{0.61}$ nanowires.[12] Both values further decrease to a minimum at -149 μV/K at 204 K, as shown in Fig. 3(d). The Seebeck coefficient as a function of temperature depends on the carrier concentration and overlaps between bulk and surface states. The characteristic dip occurs when the chemical potential crosses from the bulk conduction band into the bandgap.[22] By comparison with the data presented in Fig. 3 of Ref. 22, our nanowires are in the low-doping regime with electron charge carrier concentrations of typically on the order of $n \sim 10^{18}$ cm^{-3}. In this regime, the (temperature-independent) contribution of the topological surface state to the overall thermoelectric properties is rather pronounced.[22] However, its dominance is still limited to low temperatures, as the bulk conduction is increasing exponentially due to thermal carrier activation over the narrow bandgap. Owing to the different temperature dependencies, there is a transition from a surface-to-bulk-dominated regime, leading to a maximum value of the Seebeck coefficient of roughly -150 μV/K at $\sim$190 K. One route to improve the Seebeck coefficient would be tuning the composition by annealing.[18,23,24] To conclude this section about the thermoelectric properties, we calculate the power factors from $S^2\sigma$ to (26 ± 2) μW/K^2 cm (Au-catalyzed)

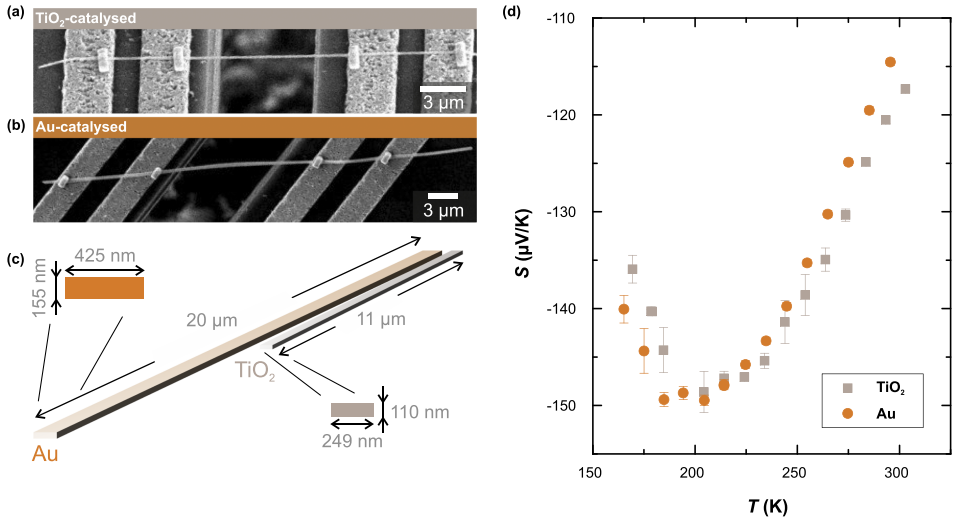

FIG. 3. [(a) and (b)] SEM micrographs of TiO_2- and Au-catalyzed Bi_2Te_3 nanowires suspended on the two cantilevers of a thermoelectric characterization platform for nanowires.[25] The nanowires are pinned down to the platform by Pt contacts deposited by electron beam deposition. The two inner electrodes measure the voltage and the two outer electrodes are used as a feedback for the heating electrodes (not shown). (c) Dimensions of the two nanowires. The Au-catalyzed nanowire is (20.1 ± 1) μm long, (155 ± 7) nm high, and (425 ± 7) nm broad. The TiO_2-catalyzed nanowire is (11.1 ± 1) μm long, (110 ± 13) nm high, and (249 ± 9) nm broad. (d) The Seebeck coefficient S as a function of temperature T is almost identical for the Au- and TiO_2-catalyzed nanowire.

and (23 ± 3) $\mu W/K^2$ cm (TiO_2-catalyzed), respectively. The power factors are comparable within the error range.

In summary, we have studied the influence of defects on the thermoelectric properties of Bi_2Te_3 nanostructures. Using two different catalysts, we are able to synthesize nanostructures that either consist purely of Bi_2Te_3 quintuple layers or also contain extended defects in the form of septuple layer Bi_3Te_4. Atomically resolved electron microscopy in combination with focused ion beam milling was employed to study the nanostructures in cross section and identify the septuple layers. These defects have an influence on the electronic properties as they locally provide *n*-type doping. Surprisingly, the influence of the commonly overlooked defects on the thermoelectric properties is rather marginal. Our work may lead to a deeper understanding and further optimization of thermoelectric nanowires, by being able to rule out the contribution of septuple layer defects and catalyst incorporation to the thermoelectric properties.

We gratefully acknowledge funding from the European Union Seventh Framework Programme under Grant Agreement No. 312483—ESTEEM2 (Integrated Infrastructure Initiative I3) and transnational access to MPI-FKF (WP13). P.S. acknowledges partial funding by EPSRC and Corpus Christi College (University of Oxford), and F.Z. acknowledges support by USTC's summer internship program. D.K. and S.F.F. gratefully acknowledge partial financial support by DFG SPP1386, Z. Wang, M. Kroener, and P. Woias for providing the TE characterization platform and O. Chiatti for help with SEM measurements. RCaH is acknowledged for their hospitality.

[1] H. J. Goldsmid, A. R. Sheard, and D. A. Wright, Br. J. Appl. Phys. **9**, 365 (1958).
[2] D.-X. Qu, Y. S. Hor, J. Xiong, R. J. Cava, and N. P. Ong, Science **329**, 821 (2010).
[3] M. S. Dresselhaus, G. Dresselhaus, X. Sun, Z. Zhang, S. B. Cronin, and T. Koga, Phys. Solid State **41**, 679 (1999).
[4] J. Zhou, C. Jin, J. H. Seol, X. Li, and L. Shi, Appl. Phys. Lett. **87**, 133109 (2005).
[5] A. Mavrokefalos, A. L. Moore, M. T. Pettes, L. Shi, W. Wang, and X. Li, J. Appl. Phys. **105**, 104318 (2009).
[6] A. I. Hochbaum and P. Yang, Chem. Rev. **110**, 527 (2010).
[7] P. Schönherr, T. Tilbury, H. Wang, A. A. Haghighirad, V. Srot, P. A. van Aken, and T. Hesjedal, Cryst. Growth Des. **16**, 6961 (2016).
[8] D. Mitchell, Microsc. Res. Tech. **71**, 588 (2008).
[9] K. Flöhr, M. Liebmann, K. Sladek, H. Y. Günel, R. Frielinghaus, F. Haas, C. Meyer, H. Hardtdegen, T. Schäpers, D. Grützmacher, and M. Morgenstern, Rev. Sci. Instrum. **82**, 113705 (2011).
[10] Z. Wang, S. S. Adhikari, M. Kröner, D. Kojda, R. Mitdank, S. F. Fischer, W. Töllner, K. Nielsch, and P. Woias, in *2013 IEEE 26th International Conference on Micro Electro Mechanical Systems (MEMS)* (IEEE, 2013), pp. 508–511.

[11] M. M. Shawrav, P. Taus, H. D. Wanzenboeck, M. Schinnerl, M. Stöger-Pollach, S. Schwarz, A. Steiger-Thirsfeld, and E. Bertagnolli, Sci. Rep. **6**, 34003 (2016).
[12] D. Kojda, R. Mitdank, A. Mogilatenko, W. Töllner, Z. Wang, M. Kröner, P. Woias, K. Nielsch, and S. F. Fischer, Semicond. Sci. Technol. **29**, 124006 (2014).
[13] P. Schönherr, L. J. Collins-McIntyre, S. Zhang, P. Kusch, S. Reich, T. Giles, D. Daisenberger, D. Prabhakaran, and T. Hesjedal, Nanoscale Res. Lett. **9**, 127 (2014).
[14] S. Breuer, C. Pfüller, T. Flissikowski, O. Brandt, H. T. Grahn, L. Geelhaar, and H. Riechert, Nano Lett. **11**, 1276 (2011).
[15] P. Schönherr, D. Prabhakaran, W. Jones, N. Dimitratos, M. Bowker, and T. Hesjedal, Appl. Phys. Lett. **104**, 253103 (2014).
[16] Y. Jiang, Y. Wang, J. Sagendorf, D. West, X. Kou, X. Wei, L. He, K. L. Wang, S. Zhang, and Z. Zhang, Nano Lett. **13**, 2851 (2013).
[17] D. L. Medlin, K. J. Erickson, S. J. Limmer, W. G. Yelton, and M. P. Siegal, J. Mater. Sci. **49**, 3970 (2014).
[18] B. Hamdou, J. Kimling, A. Dorn, E. Pippel, R. Rostek, P. Woias, and K. Nielsch, Adv. Mater. **25**, 239 (2013).
[19] G. S. Nolas, J. Sharp, and J. Goldsmid, *Thermoelectrics: Basic Principles and New Materials Developments* (SSBM, 2013), Vol. 45.
[20] D. Kojda, R. Mitdank, S. Weidemann, A. Mogilatenko, Z. Wang, J. Ruhhammer, M. Kroener, W. Töllner, P. Woias, K. Nielsch, and S. F. Fischer, Phys. Status Solidi A **213**, 557 (2016).
[21] M. C. Shaughnessy, N. C. Bartelt, J. A. Zimmerman, and J. D. Sugar, J. Appl. Phys. **115**, 063705 (2014).
[22] F. Rittweger, N. F. Hinsche, P. Zahn, and I. Mertig, Phys. Rev. B **89**, 035439 (2014).
[23] J. P. Fleurial, L. Gailliard, R. Triboulet, H. Scherrer, and S. Scherrer, J. Phys. Chem. Solids **49**, 1237 (1988).
[24] J. Lee, J. Kim, W. Moon, A. Berger, and J. Lee, J. Phys. Chem. C **116**, 19512 (2012).
[25] Z. Wang, D. Kojda, N. Peranio, M. Kröner, R. Mitdank, W. Töllner, K. Nielsch, S. F. Fischer, S. Gutsch, M. Zacharias, O. Eibl, and P. Woias, Nanotechnology **26**, 125707 (2015).